Water Research 195 (2021) 116940

Contents lists available at ScienceDirect

Water Research

journal homepage: www.elsevier.com/locate/watres

Micropollutants as internal probe compounds to assess UV fluence and hydroxyl radical exposure in UV/H_2O_2 treatment

Robin Wünsch[a,b], Carina Mayer[a,c,1], Julia Plattner[d], Fabienne Eugster[d,2], Richard Wülser[d], Jens Gebhardt[e], Uwe Hübner[f], Silvio Canonica[g], Thomas Wintgens[a,3], Urs von Gunten[b,g,*]

[a] FHNW University of Applied Sciences and Arts Northwestern Switzerland, School of Life Sciences, Institute for Ecopreneurship, Hofackerstr. 30, 4132, Muttenz, Switzerland
[b] School of Architecture, Civil and Environmental Engineering (ENAC), Ecole Polytechnique Fédérale de Lausanne (EPFL), 1015, Lausanne, Switzerland
[c] RWTH Aachen University, Aachener Verfahrenstechnik, Chemical Process Engineering, Forckenbeckstrasse 51, 52074, Aachen, Germany
[d] IWB (Industrielle Werke Basel), Margarethenstrasse 40, 4002, Basel, Switzerland
[e] Xylem Services GmbH, Boschstraße 4, 32051, Herford, Germany
[f] Chair of Urban Water Systems Engineering, Technical University of Munich, Garching, Germany
[g] Eawag, Swiss Federal Institute of Aquatic Science and Technology, Überlandstrasse 133, 8600, Dübendorf, Switzerland

ARTICLE INFO

Article history:
Received 26 October 2020
Revised 11 February 2021
Accepted 15 February 2021
Available online 18 February 2021

Keywords:
OH-radical exposure
UV/H_2O_2 AOP
in-situ probe compounds
kinetic modeling
sensitivity analysis
water treatment

ABSTRACT

Organic micropollutants (MPs) are increasingly detected in water resources, which can be a concern for human health and the aquatic environment. Ultraviolet (UV) radiation based advanced oxidation processes (AOP) such as low-pressure mercury vapor arc lamp UV/H_2O_2 can be applied to abate these MPs. During UV/H_2O_2 treatment, MPs are abated primarily by photolysis and reactions with hydroxyl radicals ($^{\bullet}$OH), which are produced *in situ* from H_2O_2 photolysis. Here, a model is presented that calculates the applied UV fluence (H_{calc}) and the $^{\bullet}$OH exposure ($CT_{\bullet OH,calc}$) from the abatement of two selected MPs, which act as internal probe compounds. Quantification of the UV fluence and hydroxyl radical exposure was generally accurate when a UV susceptible and a UV resistant probe compound were selected, and both were abated at least by 50 %, e.g., iopamidol and 5-methyl-1H-benzotriazole. Based on these key parameters a model was developed to predict the abatement of other MPs. The prediction of abatement was verified in various waters (sand filtrates of rivers Rhine and Wiese, and a tertiary wastewater effluent) and at different scales (laboratory experiments, pilot plant). The accuracy to predict the abatement of other MPs was typically within ±20 % of the respective measured abatement. The model was further assessed for its ability to estimate unknown rate constants for direct photolysis ($k_{UV,MP}$) and reactions with $^{\bullet}$OH ($k_{\bullet OH,MP}$). In most cases, the estimated rate constants agreed well with published values, considering the uncertainty of kinetic data determined in laboratory experiments. A sensitivity analysis revealed that in typical water treatment applications, the precision of kinetic parameters ($k_{UV,MP}$ for UV susceptible and $k_{\bullet OH,MP}$ for UV resistant probe compounds) have the strongest impact on the model's accuracy.

Abbreviations: *A*, Pre-exponential factor [L mol^{-1} s^{-1}]; α_2, Fraction of the deprotonated form of a micropollutant at a given pH [-]; AOP, Advanced oxidation process; c, Speed of light [m s^{-1}]; $c_{0,MP}$, Concentration of a micropollutant before UV/H_2O_2 treatment [mol L^{-1}]; c_{MP}, Concentration of a micropollutant after UV/H_2O_2 treatment [mol L^{-1}]; CBD, Collimated beam device; $CT_{\bullet OH}$, Hydroxyl radical exposure [mol L^{-1} s]; DOC, Dissolved organic carbon; ε, Decadic molar absorption coefficient at 254 nm [cm^{-1}]; ε_1, Decadic molar absorption coefficient at 254 nm of the deprotonated form of a micropollutant [cm^{-1}]; ε_2, Decadic molar absorption coefficient at 254 nm of the protonated form of a micropollutant [cm^{-1}]; *E*, Ultraviolet fluence rate [W m^{-2}]; E_a, Activation energy [J mol^{-1}]; h, Planck's constant [J s]; *H*, Ultraviolet fluence [J m^{-2}]; $k_{\bullet OH}$, Second-order rate constant for the reaction with hydroxyl radicals [L mol^{-1} s^{-1}]; k_{UV}, Fluence-based rate constant for direct photolysis [m^2 J^{-1}]; λ, Wavelength [m]; N_A, Avogadro number [einstein^{-1}]; MP, Micropollutant; $^{\bullet}$OH, Hydroxyl radical; Φ, Quantum yield at 254 nm [mol einstein^{-1}]; R, Ideal gas constant [J K^{-1} mol^{-1}]; *S*, *Pseudo*-first-order hydroxyl radical scavenging rate constant of matrix [s^{-1}]; *T*, Absolute temperature [K]; TIC, Total inorganic carbon; u^2, Combined standard uncertainty [-]; u_c^2, Combined standard variance [-]; UV, Ultraviolet; UVA, Ultraviolet absorbance at 254 nm normalized to the path length [m^{-1}]; Δ%, Difference between % predicted abatement and % measured abatement [-].

* Corresponding author.
E-mail address: vongunten@eawag.ch (U. von Gunten).
[1] Present address: Nalco Deutschland GmbH, Solmsstraße 41, 60486 Frankfurt am Main, Germany.
[2] Present address: F.Hoffmann-La Roche AG, Sicherheit, Gesundheits- und Umweltschutz, Grenzacherstrasse 124, 4070 Basel, Switzerland.
[3] Present address: RWTH Aachen University, Institut für Siedlungswasserwirtschaft, Mies-van-der-Rohe-Str. 1, 52074 Aachen, Germany.

https://doi.org/10.1016/j.watres.2021.116940

1. Introduction

To mitigate the impact of organic micropollutants (MPs), advanced oxidation processes (AOPs) are a treatment option in utilities for drinking water production (Kruithof et al., 2007; Scheideler et al., 2011; Stefan, 2018; von Gunten, 2018) or (in)direct potable water reuse (Roback et al., 2019; Stefan, 2018; Trussell et al., 2019). AOPs are based on *in situ* generation of highly reactive radicals (e.g., $^{\bullet}OH$, $SO_4^{\bullet-}$), that react almost diffusion-controlled with many constituents in water (Lee et al., 2020; von Gunten, 2018). Despite the many options for radical generation, AOPs deployed in full-scale drinking water treatment are currently either ozone-based (O_3, O_3/H_2O_2) or ultraviolet (UV) radiation based (UV/H_2O_2, UV/Cl_2) (Miklos et al., 2018b). Ozone-based processes can form the possibly carcinogenic bromate (BrO_3^-), if bromide (Br^-) is present in the raw water (von Gunten, 2003). Strategies exist for the mitigation of bromate formation, however, for waters containing high concentrations of bromide in the water (> 100 μg L^{-1} (von Gunten, 2003)), the UV/H_2O_2 process is often preferred because there is no bromate formation (von Gunten and Oliveras, 1998). In addition, other considerations can lead to the selection of a UV-based AOP, if e.g., the targeted MPs are more efficiently abated by direct photolysis, as in the case of *N*-nitrosodimethylamine (NDMA) or most X-ray contrast media (Scheideler et al., 2011).

1.1. The UV/H_2O_2 process

The abatement of MPs in the UV/H_2O_2 process is based on a combination of the direct photolysis of the MP and reactions with $^{\bullet}OH$, that are formed upon photolysis of H_2O_2 (Rosenfeldt et al., 2006; Stefan, 2018). The abatement can be described as follows:

$$\ln\left(\frac{c_{0,MP}}{c_{MP}}\right) = H \times k_{UV,\,MP} + CT_{\bullet OH} \times k_{\bullet OH,MP} \quad (1)$$

$c_{0,MP}$ and c_{MP} (mol L^{-1} = M) describe the concentrations of a MP before and after the UV/H_2O_2 treatment, respectively. H is the UV fluence (J m^{-2}), $CT_{\bullet OH}$ is the $^{\bullet}OH$ exposure (M s). $k_{\bullet OH,MP}$ (M^{-1} s^{-1}) is the second-order rate constant for the reaction of a MP with $^{\bullet}OH$. $k_{UV,\,MP}$ is the fluence-based rate constant for direct photolysis of the MP (m^2 J^{-1}), which can be calculated from Eq. 2 (Bolton and Stefan, 2002):

$$k_{UV,\,MP} = \frac{\ln(10)}{10}\frac{\lambda}{hcN_A}\varepsilon\Phi \quad (2)$$

λ denotes the wavelength, i.e., 254 nm; h: Planck's constant (6.62×10^{-34} J s), c: speed of light (3×10^8 m s^{-1}), N_A: Avogadro's number (6.022×10^{23} einstein^{-1}). ε and Φ are the decadic molar absorption coefficient (M^{-1} cm^{-1}) and quantum yield (mol einstein^{-1}) at 254 nm , respectively. For some selected MPs, $k_{\bullet OH,MP}$, ε and Φ are summarized in Table 1. For reported pH-dependent values for ε, the values at the actual pH can be calculated by Eq. 3 (Canonica et al., 2008):

$$\varepsilon = \varepsilon_1 + (\varepsilon_2 - \varepsilon_1)\alpha_2 \quad (3)$$

ε_1 and ε_2 are the decadic molar absorption coefficients of the protonated and deprotonated form of a MP, respectively. The fraction of the deprotonated form of the MP at a given pH, α_2, is calculated by Eq. 4 and employing the pK_a of the MP's protonated form.

$$\alpha_2 = \frac{1}{1 + 10^{pK_a - pH}} \quad (4)$$

The pH-dependent quantum yield is calculated analogously (Canonica et al., 2008).

Second-order rate constants for the reactions of a large number of MPs with $^{\bullet}OH$ are compiled in a database (National Institute of Standards and Technology, 2002) or can be deduced theoretically (Minakata et al., 2009). Possible temperature effects on the rate constants are discussed in Section 3.1.2. Molar absorption coefficients and photolysis quantum yields are also reported in literature (Bahnmüller et al., 2015; Canonica et al., 2008; Wols et al., 2013; Wols and Hofman-Caris, 2012), however, for these parameters no simple estimations are possible.

1.2. Approaches to assess UV fluence and $^{\bullet}OH$ exposure

Commonly, a UV fluence rate E (W m^{-2}) is measured either by chemical actinometry, e.g., potassium iodide-iodate (Bolton et al., 2011; Rahn, 1997), or by previously calibrated radiometers. Chemical actinometers are based on a known photochemical reaction with a known quantum yield.

The hydroxyl radical exposure ($CT_{\bullet OH}$, M s) is commonly determined indirectly by measurement of the abatement of an $^{\bullet}OH$ probe compound, such as *para*-chlorobenzoic acid (*p*CBA) (Haag and Hoigné, 1985; Hoigné, 1997; Rosenfeldt and Linden, 2007), or a dye, such as methylene blue (Donham et al., 2014; Keen et al., 2014; Wang et al., 2020), rhodamine B (Kwon et al., 2014), or fluorescein (Donham et al., 2014). Alternatively, it can be estimated as $CT_{\bullet OH} = c_{\bullet OH,SS} \times t$, where t (s) is the reaction time and $c_{\bullet OH,SS}$ (M) is the *pseudo* steady-state concentration of $^{\bullet}OH$ obtained from given initial water quality parameters, the average H_2O_2 concentration ($\overline{c_{H_2O_2}}$, M) and the UV fluence rate (Bolton and Stefan, 2002; Lee et al., 2016; Wols and Hofman-Caris, 2012):

$$c_{\bullet OH,SS} = E \times \frac{\ln(10)}{10}\frac{\lambda}{hcN_A} \times \frac{\varepsilon_{H_2O_2} \times \Phi_{H_2O_2} \times \overline{c_{H_2O_2}}}{S + k_{\bullet OH,H_2O_2} \times \overline{c_{H_2O_2}}} \quad (5)$$

$\varepsilon_{H_2O_2}$ = ~18.6 M^{-1} cm^{-1} to 19.2 M^{-1} cm^{-1} at 254 nm (Miklos et al., 2018b; Stefan, 2018), $\Phi_{H_2O_2}$ = 1.0 (Stefan, 2018) and $k_{\bullet OH,H_2O_2} = 2.7 \times 10^7$ M^{-1} s^{-1} (Buxton et al., 1988). The *pseudo*-first-order $^{\bullet}OH$ scavenging rate constant of the background water matrix (S, s^{-1}) can be measured directly (Wang et al., 2020), or calculated from the individual contributions of the main $^{\bullet}OH$ scavengers (i), which are essentially dissolved organic carbon, carbonate and bicarbonate for surface waters:

$$S = \sum_i c_i \times k_{\bullet OH,i} \quad (6)$$

1.3. Approaches to predict micropollutant abatement

Current *a priori* approaches to predict the abatement of MPs in UV/H_2O_2 systems are often based on the above described theories, which may be coupled, for sophisticated assessments, with computational fluid dynamics methods (Crittenden et al., 1999; Minakata et al., 2017; Wols et al., 2015a, 2015b, 2014). Alternatively, empirical correlations with *online* measurements of optical water matrix parameters, such as UV absorbance or fluorescence, were suggested for indirect monitoring of the MP abatement by the UV/H_2O_2 process (Gerrity et al., 2016; Yu et al., 2015). For ozonation and ozone-based AOPs, an *a posteriori* approach was suggested, in which the measured abatement of MPs with known second-order rate constants for the reactions with O_3 and $^{\bullet}OH$ was used to predict the abatement of other MPs (Acero et al., 2000; Huber et al., 2003; Hübner et al., 2013; Lee et al., 2013; Zucker et al., 2016). The abatement of MPs by ozonation and O_3/H_2O_2 treatment in ultrapure and drinking water was successfully modelled using the aforementioned approach, and oxidant exposures were determined from the abatement of an ozone-resistant and an ozone-reactive compound (Acero et al., 2000; Huber et al., 2003). Also for wastewater ozonation, the $^{\bullet}OH$ exposure could be well determined by back-calculation from ozone-resistant compounds, such as iopromide, clofibric acid, ibuprofen,

ketoprofen or primidone (Hübner et al., 2013; Lee et al., 2013; Zucker et al., 2016). In contrast, the use of prevalent MPs as internal probe compounds to determine the ozone exposure in wastewater and subsequently model the abatement of other MPs was not successful (Hübner et al., 2013; Lee et al., 2014; Zucker et al., 2016). A mass transfer limitation related to mixing at low ozone dosages is assumed to probably be the cause for similar removal of MPs despite several orders of magnitude difference in some second-order rate constants (Hübner et al., 2013).

Lester et al. (2014) proposed sucralose as an internal probe compound to monitor full-scale UV-AOP treatments. They suggested to predict the abatement of other MPs based on empirical, water-specific correlation factors. Here, a model is presented that can be applied without prior water-specific calibration, as it is based on widely accepted, fundamental (photo)chemical reaction theories. While this approach does not provide a real-time control option, it is useful (i) to predict the abatement of MPs with known second-order rate constants for their reactions with $^{\bullet}OH$ ($k_{\bullet OH,MP}$), molar absorption coefficients at 254 nm (ε) and quantum yields at 254 nm (Φ) that were not monitored. By this, (ii) the model allows to extrapolate from indicator compounds during performance validation tests to any other compound that might appear in the source water. Further, (iii), the model allows to check the plausibility of experimental results (data consistency).

In this paper, a model based on the measured abatement of two MPs is developed for low pressure UV/H_2O_2 processes. Two main potential applications of the model are presented, (i) the assessment of UV fluence and $^{\bullet}OH$ exposure and (ii) the prediction of abatement of MPs with known (photo)chemical reactivity. The applications are verified with data from own experiments and literature representing different treatment systems (laboratory and pilot-scale) and water matrices (surface waters and a wastewater effluent). Finally, the sensitivity of the model is assessed to elucidate the most relevant experimental parameters for accurate predictions.

2. Materials and Methods

2.1. Water samples

Water samples were taken from two river water rapid sand filtrates, i.e., Rhine and Wiese in northwestern Switzerland. The production of the rapid sand filtrates is described in the Supporting Information (SI), Text S1. Sand filtrate water grab samples of the rivers Rhine and Wiese were collected for laboratory experiments in annealed glassware at different time points (May 2016 – January 2019). Samples were stored at 4°C until use and the UV/H_2O_2 experiments were conducted within seven days after sampling. A summary of characteristic water quality parameters and MP concentrations of the sand filtrates of rivers Rhine and Wiese is provided in Table 1. The MPs were selected because of their presence in the raw waters and relevance for drinking water treatment, as well as reported specific (photo)chemical and physical data, i.e., $k_{\bullet OH,MP}$, ε and Φ (see Table 1).

2.2. Experimental setup

2.2.1. Laboratory experiments

Laboratory experiments were conducted on a collimated beam device (CBD) (Bolton and Stefan, 2002) at room temperature (20°C) to verify the model under well-defined conditions. Experiments were conducted with varying H_2O_2 concentrations (0 – 8 mg L^{-1}) and UV fluences (1'900 – 8'000 J m^{-2}, low pressure mercury UV lamps irradiating almost monochromatically at 254 nm, supplied by Xylem Services) to assess the model under process conditions relevant for realistic water treatment applications. A description of the CBD experimental procedure is provided in Text S2 (SI). Details on the experimental set points in the laboratory experiments are described in Table S3 (SI) for river Rhine sand filtrate and Table S4 (SI) for river Wiese sand filtrate.

In some laboratory experiments with river Rhine sand filtrate, selected MPs were spiked for a better quantification of the abatement at elevated H_2O_2 concentrations and UV fluences. Therefore, a mix stock solution was prepared in ultrapure water with concentrations of 1 mg L^{-1} acesulfame (ACE), diatrizoic acid (DTA), iohexol (IHX), iopamidol (IPA), iopromide (IPR) and metformin (MET), and 0.5 mg L^{-1} 5-methyl-1H-benzotriazole (5BTZ) as described in Text S3 (SI). Prior to the experiment, 25 µL of this stock solution were spiked into a 250 mL water sample, thus achieving final concentrations of 100 ng L^{-1} for these MPs (exception: 50 ng L^{-1} for 5BTZ). All chemicals were of the highest available quality and used without further purification (Table S2, SI).

2.2.2. Pilot plant experiments

Pilot plant experiments were conducted to validate the model under operational conditions and at different times throughout the year. A detailed description of the pilot plant is provided in Text S4 (SI), including a scheme of the continuously operated pilot plant (average volume flow ~ 0.5 m^3 h^{-1}, Figure S3, SI). Sand filtrates from the rivers Rhine and Wiese were treated in two parallel UV/H_2O_2 units operated at 4 mg H_2O_2 L^{-1} and a UV fluence of 6'000 J m^{-2} (600 mJ cm^{-2}) (low pressure mercury UV lamp irradiating almost monochromatically at 254 nm, supplied by Xylem Services). This set point was selected because the results of CBD experiments indicated that, under these conditions, X-ray contrast media occurring in the river Rhine sand filtrate were abated by ≥ 80 %. Furthermore, such a treatment constitutes some additional "broad band barrier" for MPs due to the $^{\bullet}OH$ generation (Plattner et al., 2017). In an additional set of experiments, the operational set points were varied (0 – 10'000 J m^{-2}, 0 – 10 mg H_2O_2 L^{-1}) to verify the model at other set points relevant for water treatment. Water temperatures during the pilot trials varied in the range of 5.0 to 24.5°C. Details on the sampling dates and operational set points are described in Table S5 (SI) for river Rhine sand filtrate and Table S6 (SI) for river Wiese sand filtrate. The pilot plant data of the UV/H_2O_2 treatment of the river Rhine sand filtrate (data set numbers 31 – 42 and 48, Table S5, SI) have been presented elsewhere (Wünsch et al., 2019), but they are re-evaluated here to test the proposed model. A .csv-file with all measured micropollutant concentrations is provided in the SI.

2.3. Analytical methods

Residual H_2O_2 in all samples was quenched by addition of 2 mol sodium thiosulfate (from a stock solution) per mol H_2O_2. The sodium thiosulfate stock solution was prepared by dissolving 1.7 g $Na_2S_2O_3$ in 50 mL ultrapure water. Even though H_2O_2 quenching was not complete under these conditions (Wünsch et al., 2019), possible Fenton-like reactions of residual H_2O_2 with Fe(III) and Cu(II) present in the surface water filtrates were shown to be irrelevant in a "dark experiment" (no UV fluence) with 4 mg H_2O_2 L^{-1} at pilot scale with river Rhine and Wiese sand filtrates (Figure S4, SI).

Analytical methods for the measurements of the MPs are described in Text S3 (SI). In brief, 5-methyl-1H-benzotriazole (5BTZ), 1H-benzotriazole (BTZ), carbamazepine (CBZ), metformin (MET), metoprolol (MPL), sulfamethoxazole (SMX) and sotalol (STL) were measured on an HPLC-MS/MS system after direct injection. Acesulfame (ACE), diatrizoic acid (DTA), iohexol (IHX), iopamidol (IPA) and iopromide (IPR) were measured on the same system after 10-fold pre-concentration but employing a different set of separation columns. Details on the analytical measurement uncertainties of

Table 1
Water quality parameters of rapid sand filtrates of rivers Rhine and Wiese (average ± standard deviation). Data base: 14 (Rhine sand filtrate) and 13 (Wiese sand filtrate) grab samples taken between June 2017 and April 2019, unless stated otherwise. Data of the river Rhine sand filtrate from June 2017 to August 2018 have been presented before (Wünsch et al., 2019), but are included here to evaluate the model with an extended data set. Concentrations of selected micropollutants and their relevant physico-chemical properties are also shown as average ± standard deviation. $k_{\bullet OH,MP}$ is the second-order rate constant for the reaction of a micropollutant with $^{\bullet}OH$ and is generally assumed to have a limited pH dependence. For reported pH-dependent photophysical properties, subscripts '1' and '2' are the respective parameters of the protonated and deprotonated form of a MP, respectively. ε is the decadic molar absorption coefficient at 254 nm; ε_1 and ε_2 are the decadic molar absorption coefficients at 254 nm of the protonated or deprotonated form of a micropollutant, respectively; Φ is the quantum yield at 254 nm; Φ_1 and Φ_2 are quantum yields at 254 nm of the protonated or deprotonated form of a micropollutant, respectively.

Parameter	Unit	Rhine sand filtrate	Wiese sand filtrate	Molecular weight (g mol^{-1})	pK_a	$k_{\bullet OH,MP}$ / 10^9 M^{-1} s^{-1}	ε or ε_1 (M^{-1} cm^{-1})	Φ or Φ_1 (mol einstein^{-1})	ε_2 (M^{-1} cm^{-1})	Φ_2 (mol einstein^{-1})
Dissolved organic carbon (DOC)	mg L^{-1}	1.4±0.3[I]	1.3±0.4[II]	-	-	2.3 × 10^4 L mgC^{-1} s^{-1},[u]	-	-	-	-
Total inorganic carbon (TIC)	mg L^{-1}	28.5±5.1[III]	12.9±4.1[IV]	-	HCO_3^-: 6.35 CO_3^{2-}: 10.33	0.0085[v] 0.39[v]	-	-	-	-
pH	-	8.1±0.1	7.8±0.2	-	-	-	-	-	-	-
UV absorbance at 254 nm divided by path length (UVA)	m^{-1}	3.5±0.8	4.4±1.1	-	-	-	-	-	-	-
Temperature (T)	°C	14.9±6.7	14.1±7.2	-	-	-	-	-	-	-
Nitrate	mg L^{-1}	5.5±1.5[V]	4.7±0.8[VI]							
5-Methyl-1H-benzotriazole (5BTZ)	ng L^{-1}	26±9	22±20	133.2	8.5±0.3[a]	8.71±0.06[a]	5230±77[a]	0.016±0.001[a]	3440±153[a]	0.0049±0.0008[a]
Acesulfame (ACE)	ng L^{-1}	244±87	79±30	163.2	~2.0[b]	3.8±0.3[c]	3600[d]	0.187[d]	-	-
1H-Benzotriazole (BTZ)	ng L^{-1}	176±41	230±142	119.1	8.3±0.2[a]	8.3±0.2[a]	6140±97[a]	0.016±0.001[a]	4500±301[a]	0.0026±0.0003[a]
Carbamazepine (CBZ)	ng L^{-1}	4±10	17±17	236.3	16.0[e]	8.0±1.9[f]	6070[g]	0.00060±0.00009[g]	-	-
Diatrizoic acid (DTA)	ng L^{-1}	26±7	37±26	613.9	2.2[e]	0.59±0.06[j]	19000±818[k]	0.039±0.002[k]	-	-
Iohexol (IHX)	ng L^{-1}	31±21	Not detected	821.1	11.7[e]	3.5±0.4[L]	27620[g]	0.04030±0.00009[g]	-	-
Iopamidol (IPA)	ng L^{-1}	193±129	Not detected	777.1	10.7[m]	3.4±0.3[n]	22700[o]	0.03318[o]	-	-
Iopromide (IPR)	ng L^{-1}	112±50	Not detected	791.1	11.1[e]	3.32±0.03[p]	21470±608[q]	0.034±0.008[q]	-	-
Metformin (MET)	ng L^{-1}	204±68	98±66	129.2	12.3[e]	1.4±0.1[k]	940±5[k]	0.014±0.003[k]	-	-
Metoprolol (MPL)	ng L^{-1}	5±3	19±10	267.4	9.7[e]	7.6±0.7[k]	519±318[r]	0.045±0.034[r]	-	-
Sulfamethoxazole (SMX)	ng L^{-1}	17±5	13±8	253.3	5.7[h]	5.9±1.6[r]	11890±117[i]	0.212±0.009[i]	16760±194[i]	0.046±0.011[i]
Sotalol (STL)	ng L^{-1}	3±6	11±7	272.4	8.2, 9.8[m]	7.9±1.6[s]	370±20[t]	0.39±0.02[t]	-	-

I: n = 24 (February 2017 – April 2019), II: n= 18 (February 2017 – April 2019), III: n = 18 (February 2017 – April 2019), IV: n = 15 (February 2017 – April 2019). V: Data from periodic river Rhine raw water monitoring; n = 28 (March 2017 – April 2019). VI: Data from an upstream river monitoring station, n = 28 (March 2017 – April 2019), (Landesanstalt für Umwelt Baden-Württemberg, 2021).
a: (Bahnmüller et al., 2015), b: (Froloff et al., 1998), c: (Toth et al., 2012), d: (Yu et al., 2019), e: predicted by MarvinSketch (V.19.18), ChemAxon, f: (Wols and Hofman-Caris, 2012), g: (Pereira et al., 2007), h: (Huber et al., 2003), i: (Canonica et al., 2008), j: average of reported values in (Wols et al., 2013) and (Real et al., 2009), k: average of reported values in (Wols and Hofman-Caris, 2012) and (Wols et al., 2014), L: average of reported values in (Pereira et al., 2007) and (Jeong et al., 2010), m: The Merck Index Online (www.rsc.org/merck-index/, accessed: February 12, 2020), n: (Jeong et al., 2010), o: (Tian et al., 2014), p: average of reported values in (Huber et al., 2003) and (Jeong et al., 2010), q: average of reported values in (Yu et al., 2019) and (Canonica et al., 2008), r: average of reported values in (Wols and Hofman-Caris, 2012) and (Wols et al., 2013), s: (Wols et al., 2013), t: (Wols et al., 2014), u: average value of five surface water sources (Brezonik and Fulkerson-Brekken, 1998), v: (Buxton et al., 1988).

the MPs are provided in Table S7 (SI), respective values for theoretical limits of quantification and a list of the suppliers of the chemicals in Table S2 (SI).

2.4. Model for prediction of micropollutant abatement

The proposed model is based on the assumption that the abatement of MPs during the UV/H_2O_2 process can be described by direct photolysis at 254 nm and reactions with $^{\bullet}$OH. Reactions with other reactive species, e.g., carbonate radicals ($CO_3^{\bullet-}$) , are neglected. Note that these reactions can become more important than reactions with $^{\bullet}$OH, e.g., if the ratio of the steady−state concentrations of $CO_3^{\bullet-}$ to $^{\bullet}$OH exceeds two to three orders of magnitude, and second-order rate constants for reactions of MPs with $CO_3^{\bullet-}$ are $> 1 \times 10^7$ M^{-1} s^{-1} (Canonica et al., 2005; Wols et al., 2014). In addition, it is assumed that all MPs face the same reaction conditions (e.g., no competition for $^{\bullet}$OH or UV photons between the MPs). This is justified by the high *pseudo*-first-order $^{\bullet}$OH scavenging rate constant for the water matrix (5.7×10^4 s^{-1} and 4.0×10^4 s^{-1} for average sand filtrates of river Rhine and river Wiese, respectively) as compared to the MPs (25 s^{-1} and 23 s^{-1} based on average measured concentrations of all MPs in sand filtrates of river Rhine and river Wiese, respectively), calculated with Eq. 6, respectively. MPs are assumed not to be re-formed during or after the UV/H_2O_2 treatment in the water matrix. Furthermore, it is assumed that the analyzed probe compounds represent average concentrations of the whole UV/H_2O_2 feed and effluent. Fundamentally, it is assumed that rate constants reported from experiments elsewhere are transferable to real water systems, i.e., no water matrix interactions alter the observed rate constants. Finally, it is assumed that the UV fluence has a narrow distribution, i.e., H in Eqs. 1 and 7 is assumed to be relatively constant throughout the entire flow travelling across the UV reactor, which should be valid for laboratory experiments conducted on collimated beam devices and for typical water treatment systems with well-designed UV reactors. Under these conditions, the abatement of MPs can be described by Eq. 1.

To predict the abatement of MPs in one experimental data set, two MPs (denoted by the subscripts '1' and '2' in the following equations) are selected as internal probe compounds. Their abatements are inserted into Eq. 1 to obtain the calculated UV fluence H_{calc} and the calculated $^{\bullet}$OH exposure $CT_{\bullet OH,calc}$. Solving the corresponding system of two linear equations for H_{calc} and $CT_{\bullet OH,calc}$, yields:

$$H_{calc} = \frac{\ln\left(\frac{c_{0,1}}{c_1}\right) - \ln\left(\frac{c_{0,2}}{c_2}\right)\frac{k_{\bullet OH,1}}{k_{\bullet OH,2}}}{k_{UV,1} - k_{UV,2}\frac{k_{\bullet OH,1}}{k_{\bullet OH,2}}} \quad (7)$$

$$CT_{\bullet OH,calc} = \frac{\ln\left(\frac{c_{0,2}}{c_2}\right) - \ln\left(\frac{c_{0,1}}{c_1}\right)\frac{k_{UV,2}}{k_{UV,1}}}{k_{\bullet OH,2} - k_{\bullet OH,1}\frac{k_{UV,2}}{k_{UV,1}}} \quad (8)$$

where $c_{0,1}$ and $c_{0,2}$ are the initial and c_1 and c_2 the transient concentrations of MP1 and MP2, respectively, $k_{\bullet OH,1}$ and $k_{\bullet OH,2}$the respective second-order rate constants for the reactions of the MPs with $^{\bullet}$OH; and $k_{UV,1}$ and $k_{UV,2}$ the respective rate constants for direct photolysis of the MPs. The internal probe compounds should be selected based on different predominant abatement mechanisms. Mathematically, this corresponds to the condition that $k_{\bullet OH,1}/k_{UV,1}$ has to be clearly different from $k_{\bullet OH,2}/k_{UV,2}$, which prevents the denominators of Eqs. 7 and 8 to be close to zero. This increases the robustness of the method against analytical uncertainty. Ideally, MP '1' – the UV susceptible probe compound – is abated predominantly by UV irradiation, whereas MP '2' – the UV resistant $CT_{\bullet OH}$ probe compound – predominantly by reactions with $^{\bullet}$OH. Knowing H_{calc} and $CT_{\bullet OH,calc}$, the expected abatement of all other MPs with known $k_{\bullet OH,MP}$, ε_{MP} and Φ_{MP} can be calculated by Eq. 1.

To estimate the confidence intervals of H_{calc}, $CT_{\bullet OH,calc}$ and the predicted abatements, the uncertainties of all relevant influencing factors (i.e., pH, photochemical parameters, second-order rate constants for reactions with $^{\bullet}$OH, analytical measurement uncertainties) are accounted for in a Monte Carlo simulation by repeated calculations of H_{calc}, $CT_{\bullet OH,calc}$ and predicted abatements with each experimental data set 10^4 times. According to (Morgan et al., 1990), this is sufficient to have 95 % confidence that the actual 50th percentile is within the estimated 49th and 51st percentiles for any distribution. In each repeated calculation, the input parameters were assigned a random value around the measured value within the respective uncertainty, as described in Table S8 (SI). The confidence intervals were evaluated after the repeated calculations by evaluating the 2.5 and 97.5 percentile values of H_{calc}, $CT_{\bullet OH,calc}$ and the predicted abatements, respectively.

H_{calc} and $CT_{\bullet OH,calc}$ could also be obtained by linear regression analysis using Eq. 1 and the abatement data of more than two probe compounds. This approach can potentially make the determination of these key parameters more robust against inaccuracies of kinetic parameters and analytical errors of single substances but was not tested within this study.

2.5. Sensitivity analysis

The sensitivities of the model outputs H_{calc} and $CT_{\bullet OH,calc}$ were assessed by the Gaussian error propagation. For a model output y as a function g of $i = 1, 2, 3, \ldots N$ non-correlated input variables $x_1, x_2, x_3, \ldots x_N$

$$y = g(x_1, x_2, x_3, \ldots, x_N) \quad (9)$$

the combined variance $u_c^2(y)$ can be approximated by Eq. 10, neglecting higher-order terms in a Taylor series expansion (ISO/IEC, 2008):

$$u_c^2(y) \approx \sum_{i=1}^{N}\left(\frac{\partial g}{\partial x_i}\right)^2 \times u^2(x_i) \quad (10)$$

$u^2(x_i)$ is the estimated standard uncertainty of an input variable x_i.

The partial derivatives $\frac{\partial g}{\partial x_i}$ for H_{calc} and $CT_{\bullet OH,calc}$ were computed by an online software (Wolfram Alpha LLC, 2020) and are given in Tables S9 and S10 (SI), respectively. Standard uncertainties of second-order rate constants are assumed to be uniformly distributed, wherefore $u^2(x_i)$ becomes (ISO/IEC, 2008)

$$u^2(x_i) = \frac{(a_+ - a_-)^2}{12} \quad (11)$$

where, a_+ and a_- denote the upper and lower limits of the interval of uncertainty. For the sensitivity analysis, $u^2(x_i)$ of all kinetic constants was calculated with Eq. 11 with the assumption that kinetic constants are certain within a factor 2, i.e., a_+ as 2 $\times$ the kinetic constant and a_- as 0.5 $\times$ the kinetic constant, respectively.

A comparison of the estimated combined standard uncertainty $u_c(y) = \sqrt{u_c^2(y)}$ from the Gaussian error propagation with the results obtained from the Monte Carlo simulation (section 2.4) validated that higher-order terms of the Taylor series expansion were of minor importance.

3. Results and discussion

3.1. Prediction of abatement of micropollutants

3.1.1. Laboratory experiments: Proof of concept with sand filtrate waters of rivers Rhine and Wiese

Fig. 1 shows the predicted and measured relative abatements of the selected MPs based on the model described with IPA and 5BTZ

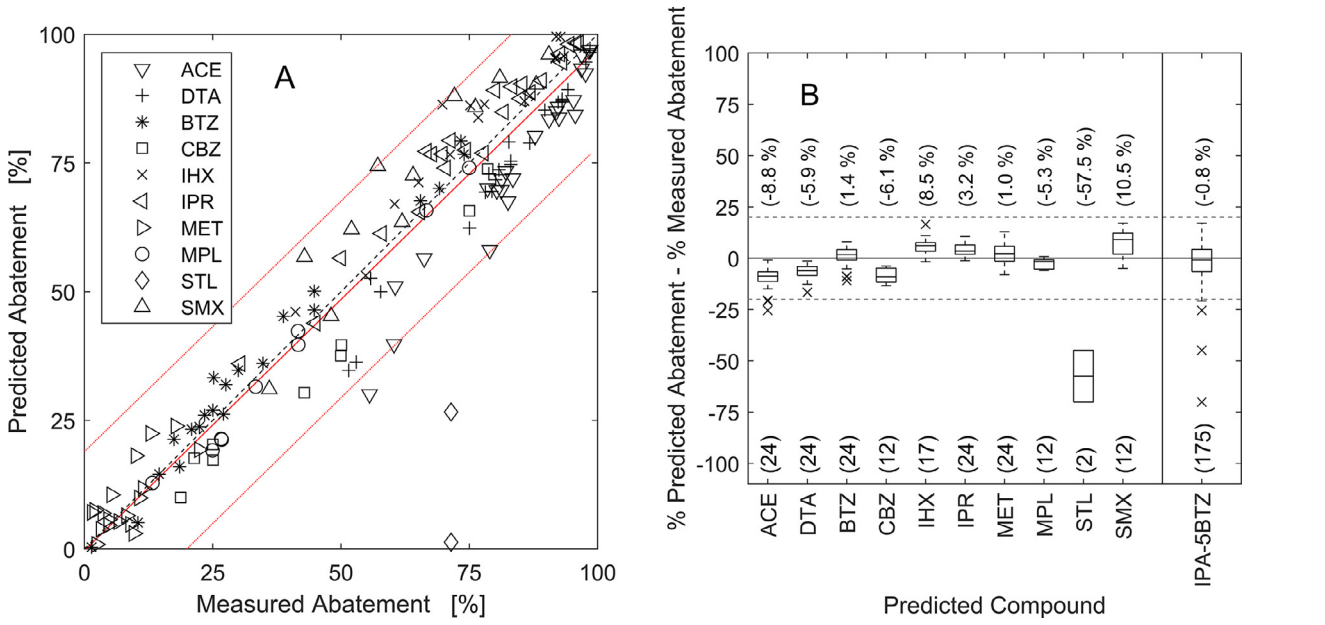

Fig. 1. Predicted abatement of selected micropollutants by the probe compound combination iopamidol (IPA) and 5-methyl-1H-benzotriazole (5BTZ) in CBD laboratory experiments with river Rhine sand filtrate. A: Predicted relative abatement in comparison to the measured relative abatement. Dashed black line: ideal model. Red lines: linear fit with 95 % confidence intervals. B: Box plots for the micropollutant-specific evaluation of the differences between the predicted and measured abatement (Δ%). The separate IPA-5BTZ box plot on the far right summarizes all box plots of the single micropollutants of the IPA-5BTZ model. Lower numbers in brackets: number of experiments with predictions for the respective micropollutant. Upper numbers in brackets: median values for Δ%. Grey dashed lines show ±20 %. ACE, DTA, BTZ, CBZ, IHX, IPR, MET, MPL, STL, SMX: acesulfame, diatrizoic acid, 1H-benzotriazole, carbamazepine, iohexole, iopromide, metformin, metoprolol, sotalol, sulfamethoxazole, respectively.

as internal probe compounds for river Rhine sand filtrate. The presented data are based on 24 CBD experiments, including six experiments without H_2O_2 addition (H_{set} = 1'900 – 8'000 J m^{-2}, H_2O_2 dose = 0 – 8 mg L^{-1}, data sets 1 – 24, Table S3, SI. H_{set} is the UV fluence intended to be transferred to the sample). The combination of IPA and 5BTZ was selected, because it was found to reproduce well the set UV fluence H_{set} in laboratory experiments (Fig. 2), could be applied in many cases due to high detection frequencies in the river Rhine sand filtrate (Table 1) and has the lowest median value of the difference between % predicted and % measured abatement (Δ% = -0.8%, Fig. 3) of all investigated combinations of probe compounds.

Overall, the IPA-5BTZ model predicts abatements with a Δ% within ±20% for 170 out of 175 data points (97 %, Fig. 3). Five data points are outside this range, i.e., the two predictions for sotalol and three for acesulfame. These compounds are discussed later in the manuscript. The accuracy of predictions is constant over the investigated range of UV fluences and H_2O_2 concentrations.

Especially the Δ% values of BTZ, IPR, and MET are mostly very small (< 5%), with median values of -1.4 %, 3.2 % and 1.0 %, respectively. For BTZ and IPR, this might be explained by their similar $k_{•OH}$ and k_{UV} compared to the applied probe compounds. MET mainly reacted with $^{•}$OH and was hardly abated under the investigated treatment conditions (< 25 %); hence, small values of Δ% are expected.

Predictions of STL concentrations were unsatisfactory, not only with the IPA-5BTZ model, but also with all other combinations of probe compounds (Fig. 3). STL was present only at very low concentrations in the filtrates, i.e., 7 ng L^{-1} and 4 ng L^{-1} in Rhine and Wiese, respectively. This is above the theoretical limit of quantification (1.6 ng L^{-1}, Table S7, SI) but outside the lower measurement range (10 ng L^{-1}, Table S7, SI). For this reason, analytical difficulties likely contribute to the unsatisfactory predictions. However, the observed under-predictions of STL abatement by the model could also result from disregarded reactions with $CO_3^{•-}$, which were reported to react with STL with a second-order rate constant of (2.2±1.7) × 10^8 M^{-1} s^{-1} (Wols et al., 2014). Assuming

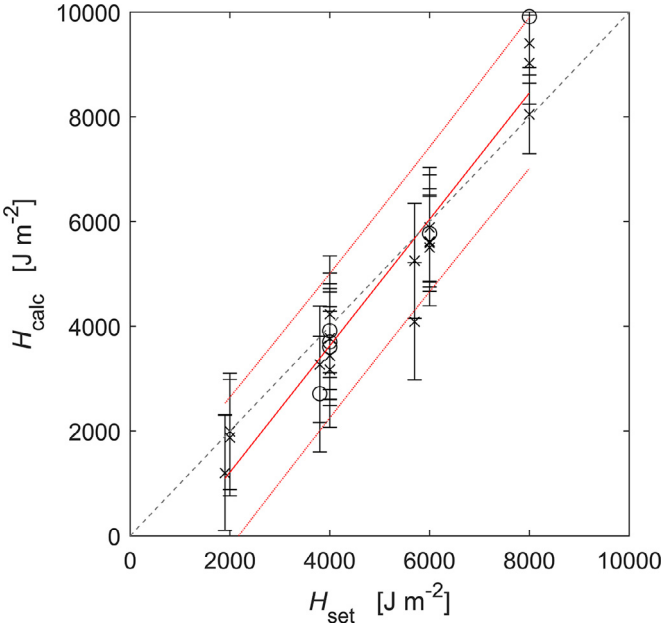

Fig. 2. Calculated UV fluence (H_{calc}) in comparison to the set UV fluence (H_{set}). Probe compounds: iopamidol and 5-methyl-1H-benzotriazole. Data set: CBD laboratory experiments with river Rhine sand filtrate (set numbers: 1 – 24, Table S3, SI). Circles show experiments without H_2O_2 addition, crosses with H_2O_2 addition. Error bars represent 95 % confidence intervals. Dashed black line: ideal model. Red lines: Linear fit with 95 % confidence interval.

that the $CO_3^{•-}$ exposure is about two to three orders of magnitude higher than the $^{•}$OH exposure (Canonica et al., 2005), the expected ln abatement by reactions with $CO_3^{•-}$ is about 3- to 30-fold higher than the abatement *via* $^{•}$OH.

The CBD experiments with sand filtrates of rivers Rhine and Wiese were used to assess the significance of H_{calc}. H_{calc} and H_{set} correlated well in the laboratory experiments, as expected (Fig. 2,

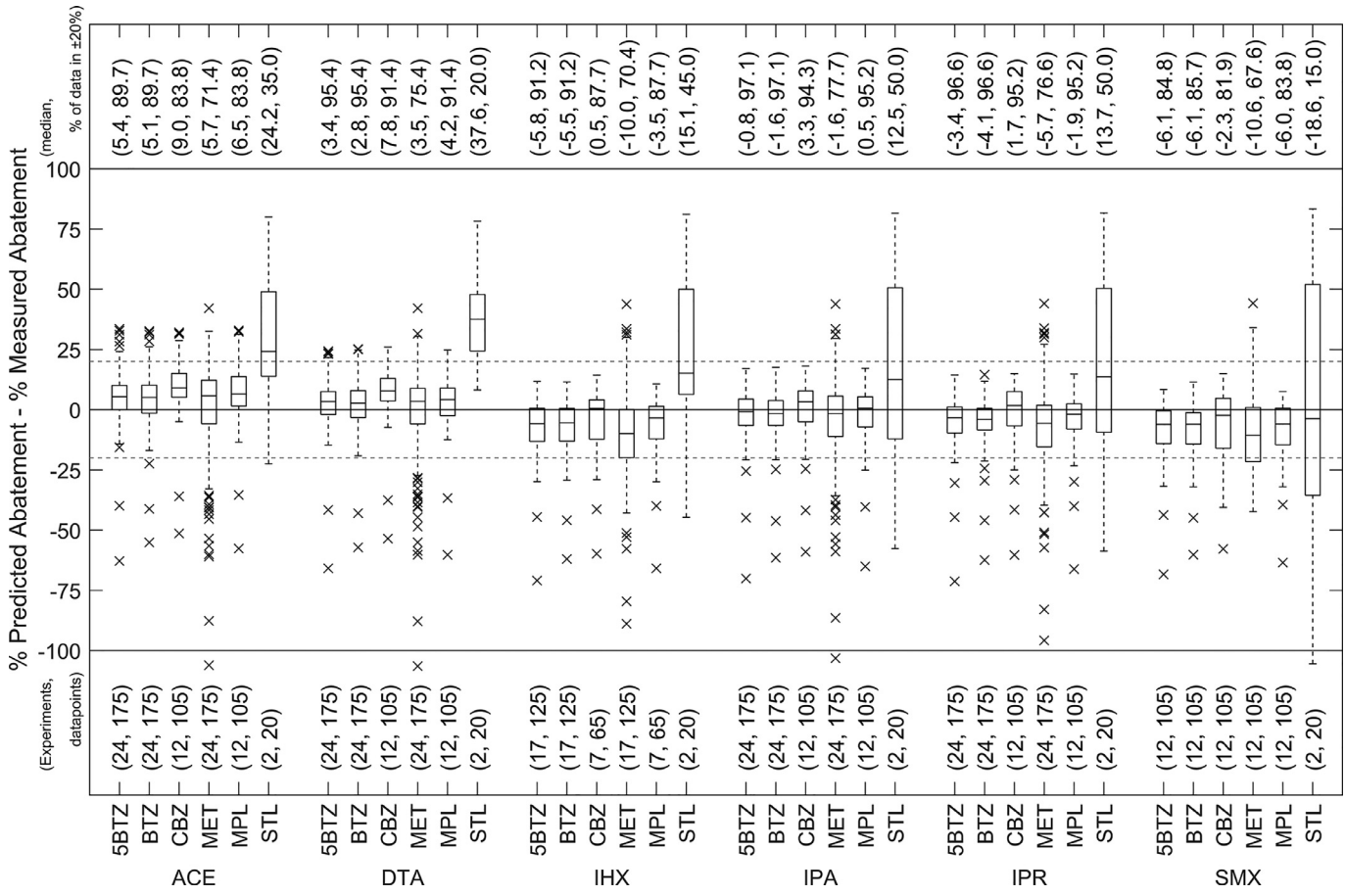

Fig. 3. CBD laboratory experiments with river Rhine sand filtrate: Overview on differences between predicted and measured % abatement of possible combinations of probe compounds (Δ%). Values in lower brackets: number of evaluated experiments, total number of predictions. Values in upper brackets: median of data points, share of data inside the ±20 % range, shown by gray dashed lines. Horizontal names: UV susceptible probe compound, i.e., ACE, DTA, IHX, IPA, IPR, SMX: acesulfame, diatrizoic acid, iohexol, iopamidol, iopromide, sufamethoxazole, respectively. Vertical names: UV resistant $CT_{\bullet OH}$ probe compound, i.e., 5BTZ, BTZ, CBZ, MET, MPL, STL: 5-methyl-1H-benzotriazole, 1H-benzotriazole, carbamazepine, metformin, metoprolol, sotalol, respectively.

combination of IPA and 5BTZ). From 24 assessed data sets, 95 % confidence intervals of H_{calc} of only four data sets did not include H_{set}, i.e., data sets 1, 2, 3 and 24 (Table S3, SI). The first three data sets were all conducted with the same water sample, which might indicate a systematic experimental error for this series of experiments. This showcases the potential application of the model to check the consistency of experimental data.

Depending on the choice of the photo-sensitive probe compound, H_{calc} was found either higher or lower than H_{set} (Table S11, SI). Small differences between H_{calc} and H_{set} were found for all combinations of probe compounds that used DTA, IHX, IPA or IPR as UV probe compound, except when STL was selected as the $CT_{\bullet OH}$ probe compound. It can be concluded that H_{calc} can reproduce H_{set}, if a suitable combination of probe compounds is selected.

Fig. 3 provides an overview of the prediction quality of all investigated combinations of internal probe compounds in laboratory experiments with sand filtrate of the river Rhine. For example, Δ% of all models with ACE as a probe compound are grouped in the first block (far left) of Fig. 3. The second probe compound is indicated in vertical text above the ACE label. The first boxplot shows results based on ACE and 5BTZ as probe compounds. Like the boxplot on the far right of Fig. 1, one boxplot summarizes the prediction accuracy for the abatement of all other MPs (i.e., ACE and 5BTZ excluded) discussed in this paper. The number of distinct experiments and prediction results in each boxplot is indicated in vertical at the lower x-axis. The boxplot for ACE and 5BTZ as probe compounds represents 175 prediction results of DTA, IHX, IPA, IPR, SMX, BTZ, CBZ, MET, MPL and STL from 24 distinct laboratory experiments. At the upper x-axis, median values of Δ% are indicated and the percentage of Δ% inside the ±20 % boundaries.

For most combinations of probe compounds, the prediction quality of the model was satisfactory, i.e., the predicted abatement of MPs was mostly within ±20 % of the measured abatement. Similar results were obtained for river Wiese sand filtrate (Figure S5, SI). Therefore, it can be concluded that the model generally works well in surface water sand filtrates to predict the abatement of other substances, based on the measured abatement of two probe compounds and the available kinetic information (k_{UV} and $k_{\bullet OH}$).

A statistical assessment of the percentage of Δ% inside the ±20 % boundaries of all probe compounds in both filtrates showed that the average of all predictions is in the range of 68 % to 80 % with 95 % confidence, regardless of the choice of probe compounds (Table S12, SI). However, STL performed significantly ($p < 0.05$) worse than the others, likely for the reasons discussed above. Also MET and SMX both showed a poorer average prediction performance when used as probe compounds, respectively, although statistically not significant ($p > 0.05$). Excluding MET, SMX and STL as probe compounds from the statistical evaluation, the average percentage of Δ% inside the ±20 % boundaries was in the range of 87 % to 92 % with 95 % confidence. Only predictions with ACE as probe compound were poorer on average, but not statistically significant ($p > 0.05$). In the later evaluation, IPA and IPR performed significantly better ($p < 0.05$) than the average. The UV re-

sistant $CT_{\bullet OH}$ probe compounds 5BTZ, BTZ, CBZ and MPL performed equally well.

MET was not well suited as probe compound under the treatment conditions investigated due to low % abatement measured in the range of -8 % to 22 % only. At low values of abatement, the model is very sensitive for analytical errors, as further discussed below (section 3.3). Negative values for % measured abatement are explained by analytical measurement uncertainties, which are relatively high for MET, i.e., standard uncertainty is 19 % (Table S7, SI). In these cases, it can happen that % predicted abatements are negative, which causes an increase of the predicted MP concentration. In some cases, at the same time the % measured abatement was (strongly) positive, which explains results even below -100 % difference in Fig. 3.

When SMX was used as UV probe compound, % abatement predictions tended to be lower than the % abatement measured. Comparing H_{set} and H_{calc} in CBD experiments, the calculated UV fluence was constantly below the set value, i.e., in the range of -48 % to -34 % (combination with STL excluded, Table S11, SI). It is hypothesized that the literature value for $k_{UV,SMX}$ used in this study was too high (see also Table 2). This concurs with the previously observed reduction in $k_{UV,SMX}$ in real river water matrices compared to ultrapure water solutions (Canonica et al., 2008) and might indicate that dissolved organic matter partly inhibits the photochemical transformation of SMX by reduction of transformation intermediates back to the parent compound (Wenk et al., 2011). Of note, SMX was reported to react with $CO_3^{\bullet-}$ with a second-order rate constant of $(1.2\pm0.7) \times 10^8$ M^{-1} s^{-1} (Wols et al., 2014), which implies that the expected ln abatement by reactions with $CO_3^{\bullet-}$ is about 2- to 20-fold higher than the abatement *via* $^{\bullet}$OH. In contrast to STL, predictions of SMX abatement are typically found within ±20 % of the measured abatement. This is explained by the rapid abatement of SMX by photolysis, which is of higher importance than the abatement *via* radical species.

Similarly, when using ACE as a probe compound, H_{calc} in CBD experiments was systematically higher than H_{set} (Table S11, SI), suggesting that $k_{UV,ACE}$ from the literature is too low (see also Table 2). This explains why the abatement of ACE was often underestimated (Fig. 1) and consequently, when using ACE as UV probe compound, abatements of UV-susceptible compounds tended to be over-predicted (Fig. 3).

3.1.2. Pilot plant: Application of the model to river Rhine and river Wiese sand filtrates

The model was applied to predict the abatement of MPs in pilot plant experiments. A comparison of the Δ% values for the investigated combinations of probe compounds is provided in Figure S6 (SI) for river Rhine sand filtrate and in Figure S7 (SI) for river Wiese sand filtrate.

An assessment of the percentage of Δ% within the ±20 % boundaries of all probe compounds in both filtrates showed no statistical differences between the mean values of the experiments performed in laboratory and pilot-scale, i.e., the average value is in the range of 74 % to 81 % with 95 % confidence (Table S13, SI). Therefore, it can be concluded that the model is also applicable to sand filtrates at pilot-scale with a similar prediction performance.

However, some differences exist for single MPs, e.g., STL (better prediction performance) or MET (lower prediction performance). This might be due to effects of varying concentrations during the pilot trials.

Another reason for the observed shifts in the prediction performance could be the influence of the water temperature on $k_{UV,MP}$ and $k_{\bullet OH,MP}$. Water temperature (6.2 to 24.5°C, Table S5, SI) is not included as an input parameter in the proposed model. Possible temperature effects, i.e., activation energies, likely differ between the investigated MPs (Wols et al., 2015b), which could explain the described discrepancies between laboratory and pilot-scale experiments. However, overall, it is concluded that the differences are not very large, because the average values of Δ% inside the ±20 % boundaries at both scales are statistically indifferent. In principle, temperature effects on the rate constants k could be accounted for by the Arrhenius equation:

$$k(T) = A \times \exp\left(-\frac{E_a}{RT}\right) \quad (12)$$

T (K) is the absolute temperature, R (8.314 J K^{-1} mol^{-1}) is the ideal gas constant, A is the pre-exponential factor, E_a (J mol^{-1}) is the activation energy. However, activation energies for the relevant reaction rate constants of the selected MPs are not available in the published literature. Note that second-order rate constants for reactions of all water matrix constituents with $^{\bullet}$OH (including $^{\bullet}$OH scavengers) may also be impacted by the water temperature, which might lead to a net effect on MP abatement lower than expected.

In addition, the implementation of temperature-dependent values for $k_{\bullet OH,MP}$ and $k_{UV,\ MP}$ is expected to improve the prediction quality of the model only moderately. This assumption is based on estimated activation energies for $k_{\bullet OH,MP}$ and $k_{UV,\ MP}$ in the range of 5 – 22 kJ mol^{-1} (Christensen et al., 1982; Elliot and Simsons, 1984; Wols et al., 2015b), which leads to a variation within a factor of 1.2 to 2.0 for the rate constants in the observed temperature range. This is in the range of uncertainty of experimentally determined kinetic parameters. Therefore, it is concluded that a temperature-independent model can be used for predictions within an accuracy of ±20 % for the water temperature ranges in this study.

3.1.3. Assessment of published data from wastewater treatment with UV/H_2O_2

Published data from UV/H_2O_2 treatment of a wastewater effluent in laboratory experiments (Miklos et al., 2019) and in a pilot plant (Miklos et al., 2018a) were assessed with the model to test its applicability in advanced wastewater treatment (Fig. 4). Laboratory experiments were conducted on a CBD with tertiary wastewater effluent (H_2O_2 0 to 12.8 mg L^{-1}; UV fluences 400 to 20'000 J m^{-2} (Miklos et al., 2019, 2018a)). A pilot plant was continuously operated with tertiary wastewater effluent at a target dose of 10 mg H_2O_2 L^{-1} and a UV fluence of 8'000 J m^{-2}. Results include data from continuous monitoring over one week at dry weather conditions and another week during a rain event (Miklos et al., 2018a). Although the publication included the abatement of a large set of MPs, only the MPs selected in the current study were evaluated (Table 1).

Fig. 4 shows the results for the probe compound combination IPR-BTZ for the prediction of CBZ, MPL, SMX and STL. The other MPs discussed here were not included in the measurements of (Miklos et al., 2019) and (Miklos et al., 2018a). IPR and BTZ were selected as probe compounds because this combination had the highest share of Δ% inside the ±20 % boundaries in the experiments with river Rhine sand filtrate.

Overall, the 95 % confidence intervals for the share of Δ% within the ±20 % boundaries of all possible combinations of probe compounds are in the range of 66 % to 82 % for CBD experiments and 68 % to 84 % for pilot plant experiments, respectively (Fig. 4 B). This means that there is no statistical evidence that the measured % MPs abatement within ±20 % in wastewater is predicted with a worse performance than in experiments with surface water, both on laboratory- and pilot-scale. In addition, there is no statistical difference between the share of Δ% inside the ±20 % boundaries at dry weather or during a rain event, evaluating the eight possible combinations of probe compounds.

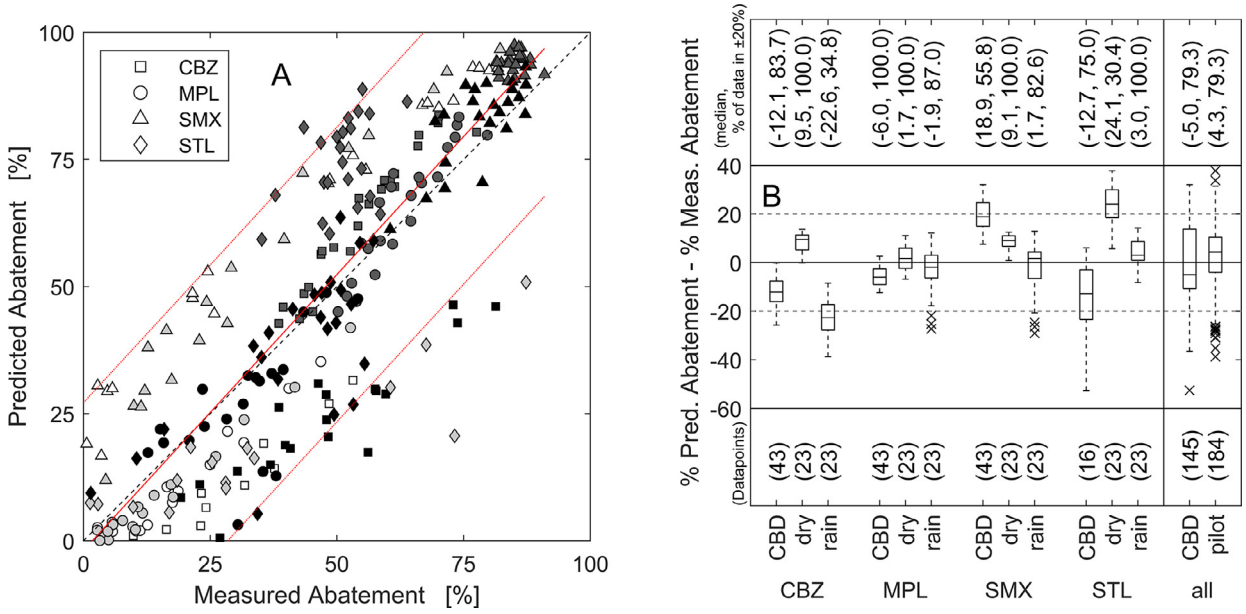

Fig. 4. Assessment of published data for UV/H_2O_2 wastewater treatment with the probe compound combination iopromide (IPR) and 1H-benzotriazole (BTZ). A: Predicted relative abatement in comparison to the measured relative abatement. White and light gray fillings: CBD experiments from Miklos et al. (2019) and Miklos et al., (2018a), respectively. Dark gray and black fillings: pilot-scale experiments at dry weather ('dry') and during a rain event ('rain'), respectively, on a continuously operated pilot plant at 10 mg H_2O_2 L^{-1}, 8'000 J m^{-2} (Miklos et al., 2018a). Dashed black line: ideal model. Red lines: linear regression with 95 % confidence intervals. B: Differences between predicted and measured % abatements from the respective micropollutants (Δ%). Lower values in brackets: number of predictions. Upper values in brackets: median and share of data inside the ±20 % boundaries, shown as gray dashed lines. Horizontal names: predicted micropollutant, i.e., CBZ, MPL, SMX, STL: carbamazepine, metoprolol, sulfamethoxazole and sotalol, respectively. Separate boxplots on the far right summarize all CBD experiments and all pilot plant experiments ('pilot') of all assessed micropollutants, respectively.

Therefore, it can be concluded that the model can be applied in a wide range of water matrices and, at least, at laboratory- and pilot-scale to predict the abatement of MPs based on the measured abatement of two MPs as internal probe compounds.

The prediction performance of the IPR-BTZ model for STL is much better in the wastewater than in the river sand filtrates. STL was present in the wastewater in the range of 32 ng L^{-1} to 83 ng L^{-1}, which was well above the limit of quantification. This contributes to the overall better results for STL, compared to the experiments with the river sand filtrates where the influent concentrations of STL were often near the limit of quantification. Note that on the pilot plant, STL abatement tended to be overpredicted, even though carbonate radicals not considered in the model should add to the predicted abatement by photolysis and $^{\bullet}$OH. The reason for this result is currently unclear and further research is necessary to fully explain this observation.

3.2. Estimation of kinetic data for micropollutants

The model was also tested for its applicability to obtain kinetic data. This can be an interesting application as a rough estimate of kinetic data that is not yet reported in literature. In a first step, the model is applied to back-calculate H_{calc} and $CT_{\bullet OH,calc}$ with Eqs. 7 and 8. In a second step, $k_{UV,MP}$ and $k_{\bullet OH,MP}$ are determined by linear regression analysis with Eq. 1, which is in principle possible if at least two experimental data points are available.

As a proof of concept, this approach was applied for well-described MPs from laboratory experiments with river Rhine sand filtrate with IPA and 5BTZ as internal probe compounds. Only positive, i.e., physically reasonable results for mean values of H_{calc} and $CT_{\bullet OH,calc}$ were used for the linear regression (data sets used: 1 – 7, 10 – 12, 14 – 18, 21 – 24, UV fluences: 1'900 – 8'000 J m^{-2}, H_2O_2: 0 – 8 mg L^{-1}, Table S3, SI). In Table 2, the fitting results of the model are compared with literature values (derived from Table 1).

Table 2
Laboratory experiments with river Rhine sand filtrate: Comparison of fitted rate constants for direct photolysis ($k_{UV,MP}$) and for reactions with $^{\bullet}$OH ($k_{\bullet OH,MP}$), along with the number of fitted data points (n), based on calculated UV fluences and $^{\bullet}$OH exposures from iopamidol and 5-methyl-1H-benzotriazole as internal probe compounds. Results show average values ± half 95 % confidence intervals for fitted kinetic parameters. Ratios compare modelled values with literature values at pH 8.1. For references of literature values, see Table 1.

Substance	n	$k_{UV,MP}$ / 10^{-4} (m^2 J^{-1})			$k_{\bullet OH,MP}$ / 10^9 (M^{-1} s^{-1})		
		Fitted	Literature [a]	k_{fitted}/k_{lit}	Fitted	Literature [b]	k_{fitted}/k_{lit}
1H-Benzotriazol (BTZ)	18	0.28±0.07	0.29	1.0	7.4±0.5	8.3	0.9
Acesulfame (ACE)	18	4.0±0.4	3.3	1.2	7.7±3.0	3.8	2.0
Carbamazepine (CBZ)	9	0.2±0.3	0.02	9.8	9.1±1.3	8.0	1.1
Diatrizoic acid (DTA)	18	4.6±0.2	3.6	1.3	0.7±1.3	0.56	1.2
Iohexol (IHX)	9	4.3±0.5	5.4	0.8	5.5±7.2	3.5	1.6
Iopromide (IPR)	18	3.2±0.2	4.0	0.8	4.5±1.6	3.3	1.4
Metformin (MET)	17	0.03±0.07	0.06	0.5	1.2±0.5	1.4	0.8
Metoprolol (MPL)	9	0.2±0.2	0.1	1.8	7.6±0.8	7.7	1.0
Sulfamethoxazole (SMX)	9	2.2±0.6	3.8	0.6	7.5±3.1	5.9	1.3

a: Values were calculated using the ε and Φ values given in Table 1 and applying Eq. 2 and, if needed, the procedure to calculate speciation-dependent ε and Φ for pH 8.1 Eqs. 3 and (4). b: Values taken from Table 1, assumed to be pH-independent.

The proposed approach leads to an agreement of predicted values for $k_{UV,MP}$ and $k_{•OH,MP}$ and those from literature within a factor 2, except for one outlier ($k_{UV,CBZ}$). This is well within the range of accuracy that can be expected for kinetic parameters which are determined experimentally by different groups (Wols and Hofman-Caris, 2012).

For some MPs, rate constants were determined with high uncertainties ($k_{UV,MP}$ of CBZ, MET and MPL, or $k_{•OH,MP}$ of DTA and IHX). Accurate estimates of rate constants are difficult to be obtained for substances that are either hardly abated by direct photolysis (CBZ, MET, MPL), or have very low values for $k_{•OH,MP}$ (DTA) (Table 1). Nevertheless, the corresponding rate constants for the main pathway, i.e., the reaction with •OH (CBZ, MET, MPL) or direct photolysis (DTA), can still be determined with good agreement with the literature. For IHX the experiments with H_{set} = 8'000 J m^{-2} were excluded for fitting, because their inclusion led to physically impossible negative values for $k_{•OH,IHX}$, likely due to analytical measurement errors at very low concentrations. The remaining data had a narrow range of $CT_{•OH,calc}$ (5.3×10^{-12} to 4.7×10^{-11} M s). This explains the large confidence interval of the estimated $k_{•OH,IHX}$ value. Furthermore, low abatement such as for MET (2 to 22 %) also leads to wide confidence intervals. Therefore, the suggested approach is only feasible if the target MP is abated to a sufficiently high extent to minimize uncertainties, e.g., from analytical measurements. Note that in principle it is also possible to estimate the *pseudo*-first-order •OH scavenging rate constant of the water matrix, *S*, from H_{calc}, CT_{calc} and Eq. 5, but the discussed limitations are also valid for this approach.

Overall, these results show some benefits to estimate rate constants, but also serious limitations. Kinetic data are typically obtained by measurements of the abatement of a selected MP under controlled laboratory conditions, at concentration levels that are high enough to reduce analytical errors, and for optimized reaction times. Whenever possible, such an approach should be adopted to determine rate constants for individual micropollutants.

3.3. Sensitivity analysis of the model

This section provides an assessment of the role of experimental parameters on the quality of the modelling results. First, the impact of the measured abatement of the probe compounds on the combined standard uncertainties (u_c) of H_{calc} and $CT_{•OH,calc}$ is assessed. In a second step, strategies to reduce the uncertainties of H_{calc} and $CT_{•OH,calc}$ are discussed, which would lead to model outputs with increased confidence. Both assessments are based on the Gaussian error propagation described before (Section 2.5).

H_{calc} and $CT_{•OH,calc}$ depend on all parameters described in Eqs. 7 and 8, i.e., concentrations of both probe compounds before and after UV/H_2O_2 treatment and their respective kinetic parameters. To reduce the complexity, only the probe compound combination IPA-5BTZ is discussed here, because it was the main combination applied in this study. Analytical measurement uncertainties for both probe compounds were 13 % in this study (Table S7, SI). The uncertainty of the rate constants was assumed within a factor 2.

Fig. 5 shows u_c of H_{calc} and $CT_{•OH,calc}$ at different levels of abatement of the probe compounds. Scenarios with a higher removal of 5BTZ compared to IPA are not of relevance for typical water treatment applications and therefore not discussed. For low relative abatements of the probe compounds (< 50%), the application of the model is not very useful, because u_c of H_{calc} and $CT_{•OH,calc}$ can exceed 100 %. In such a case, if possible, a different pair of probe compounds has to be selected, with a higher extent of abatement.

When both probe compounds are abated by at least 50 %, uncertainties of the rate constants dominate the calculations of H_{calc} and $CT_{•OH,calc}$. Independent of the operational conditions, u_c of

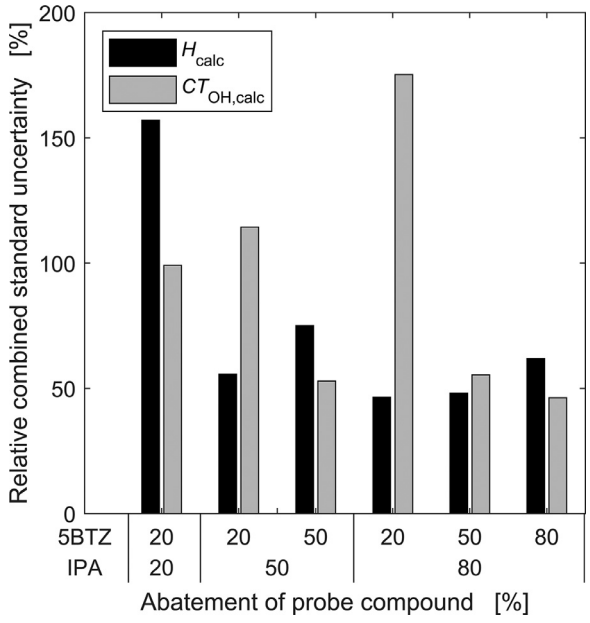

Fig. 5. Impact of different levels of abatement of the probe compounds 5-methyl-1H-benzotriazole (5BTZ) and iopamidol (IPA) on the combined standard uncertainties (u_c) of the calculated UV fluence (H_{calc}) and the calculated •OH exposure ($CT_{•OH,calc}$) relative to H_{calc} or $CT_{•OH,calc}$, respectively.

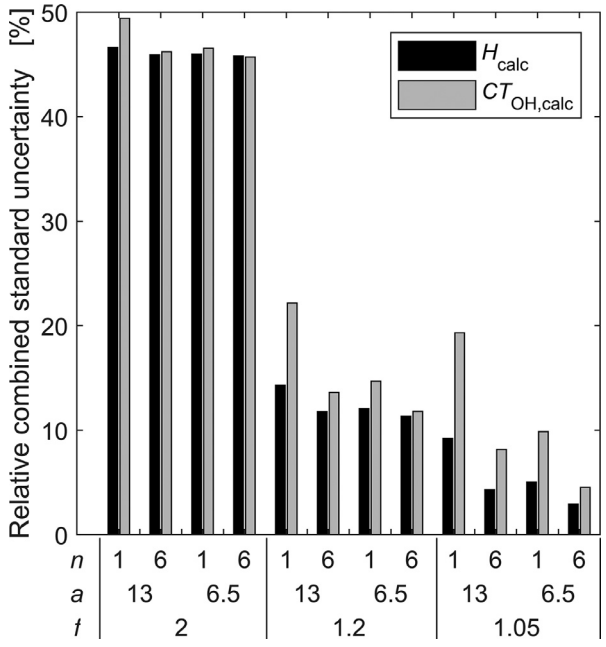

Fig. 6. Impact of strategies to minimize the relative combined standard uncertainty for the calculated UV fluence (H_{calc}) and •OH exposure ($CT_{•OH,calc}$). Model based on 93 % and 68% abatement of iopamidol (IPA) and 5-methyl-1H-benzotriazole (5BTZ) as probe compounds, respectively. *n* is the number of replicate measurements, *a* is the analytical standard uncertainty in %, *f* is the factor within which the experimentally determined rate constants are distributed around the precise value of the constants.

H_{calc} and $CT_{•OH,calc}$ cannot be reduced below 43 %, even disregarding analytical uncertainties, due to the defined uncertainty for the rate constants within a factor 2.

Impacts of several strategies to improve the model outputs, i.e., replicate measurements, improvement of analytical measurements or precision of the rate constants, are shown in Fig. 6 for IPA and 5BTZ as probe compounds. Calculations were conducted for a relatively high abatement of the probe compounds, i.e., 93 % and 68 %

for IPA and 5BTZ, respectively. These abatements result in $H_{calc} \approx$ 6'200 J m^{-2} and $CT_{\bullet OH,calc} \approx 1.1 \times 10^{-10}$ M s, which corresponds to $\approx$ 4.1 mg H_2O_2 L^{-1}, rearranging the $^{\bullet}$OH steady-state assumption (Eq. 5) and using the assumed S of an average river Rhine sand filtrate, i.e., 5.7×10^4 s^{-1}. These treatment conditions are similar to those for the long-term pilot plant study.

Under these conditions, single measurements of IPA and 5BTZ with analytical uncertainties of 13 % and rate constants uniformly distributed within a factor 2 result in u_c of 47 % and 49 % for H_{calc} and $CT_{\bullet OH,calc}$, respectively. While for H_{calc}, the uncertainty of $k_{UV,IPA}$ has the highest importance (91 % of u_c^2 of H_{calc}), $k_{\bullet OH,5BTZ}$ contributes the most to the combined variance of $CT_{\bullet OH,calc}$ (68 %). Consequently, the improvement of analytical accuracy or replicate measurements do not significantly enhance the model outputs. Therefore, an optimization can only be achieved by more precise values for the rate constants.

Kinetic parameters can be estimated within a factor 1.2 by reviewing published rate constants of several independent research groups (as done, e.g., by Buxton et al., 1988), or by using relative rate constants from one lab determined under the same treatment conditions. By this, uncertainties of rate constants limit u_c of H_{calc} and $CT_{\bullet OH,calc}$ to $\geq$ 11 %. Under these conditions, six replicate measurements can lower u_c of H_{calc} from 14 % to 12 % and u_c of $CT_{\bullet OH,calc}$ from 22 % to 14 %, respectively. Hence, replicate measurements (or improved analytical methods) can improve the predictions to some extent (especially hydroxyl radical exposure), but a considerable effort is required. At this level of precision, kinetic parameters should include temperature-dependencies (activation energies, Eq. 12), if the model is applied at other temperatures than 20 °C. Otherwise, the temperature impact on kinetic parameters can again increase the uncertainty of kinetic parameters (section 3.1.2). For u_c of H_{calc}, analytical uncertainties only play a significant role when the uncertainty of $k_{UV,IPA}$ is extremely low, i.e., accurate within a factor 1.05. With less accuracy for this rate constant, efforts to minimize analytical errors by repeated measurements or improved analytical methods are of minor relevance for H_{calc}.

4. Conclusions

A novel modeling tool based on the abatement of micropollutants acting as internal probe compounds was developed to determine the applied UV fluence and the hydroxyl radical exposure during laboratory- and pilot-scale UV/H_2O_2 treatment. This modeling approach has the advantage that water matrix parameters affecting the abatement of micropollutants (e.g., scavenging rate by background matrix, transmissivity of the water, etc.), as well as hydrodynamics and non-ideal characteristics of the UV-reactor are implicitly considered by the model. The following conclusions can be drawn:

- The model was proven to satisfactorily predict the abatement of compounds at laboratory- and pilot-scale, both for surface water sand filtrates and tertiary treated wastewater. The difference between measured and predicted abatements was typically within ±20 % for most combinations of probe compounds, even though water temperatures varied in the range of 5.0 to 24.5°C during the pilot plant experiments.
- High reactivity of substances with other radical species than $^{\bullet}$OH might limit the application of the model for certain micropollutants, especially if they are at least moderately resistant against photolysis (e.g., sotalol). For such substances, the results should be interpreted with caution, specifically in a water matrix with low contents of dissolved organic carbon or high carbonate concentrations, i.e., high ratio of $CO_3^{\bullet-}$ to $^{\bullet}$OH concentrations. *Vice versa*, if the model largely underpredicts the abatement of a substance based on photolysis and reactions with $^{\bullet}$OH, and the rate constants of the predicted substance were obtained from careful measurements in the laboratory, results might indicate significant contributions of other radical species to its abatement.
- This approach is suitable to monitor the absolute values of the UV fluence and hydroxyl radical exposure with reasonable confidence when the relative abatement of both probe compounds is at least 50 % and all rate constants are known with good precision (factor 1.2). Furthermore, concentrations of both probe compounds must be measured before and after the treatment by state-of-the-art analytical methods. When the used probe compounds are abated to a sufficiently high degree, e.g., when iopamidol and 5-methyl-1H-benzotriazole are abated by 93 % and 68%, respectively, replicate measurements or improved analytical methods do not significantly improve the model results.
- Calculated UV fluences and hydroxyl radical exposures can be used to estimate unknown rate constants (second-order rate constant for the reaction with hydroxyl radicals, fluence-based rate constant for direct photolysis). The estimated rate constants were in most cases within the common range of accuracy of published kinetic data (factor 2). However, the accuracy of this approach strongly decreases when specific reactions are very slow. Thus, this approach provides a good first estimate of rate constants but cannot substitute careful measurement of rate constants under controlled laboratory conditions.

Declaration of Competing Interest

The authors declare that they have no known competing financial interests or personal relationships that could have appeared to influence the work reported in this paper.

Acknowledgements

Pascal Temmler, Pascal Brand and their teams (all IWB) are acknowledged for their support in continuous operation and maintenance of the pilot plant and online sensors. Michael Thomann (FHNW) is acknowledged for fruitful discussions. David Miklos (TU Munich) is acknowledged for providing his original data for re-evaluation with the described model. Süleyman Yüce (RWTH Aachen University) is acknowledged for supervising the master thesis of Carina Mayer. This study was conducted within the project AquaNES, which received financial support within the European Union's Horizon 2020 program [grant agreement number 689450] and from the State Secretary for Education, Research and Innovation (SERI) of Switzerland [contract number: 16.0053-1].

Supplementary materials

Supplementary material associated with this article can be found, in the online version, at doi:10.1016/j.watres.2021.116940.

References

Acero, J.L., Stemmler, K., von Gunten, U., 2000. Degradation kinetics of atrazine and its degradation products with ozone and OH radicals: A predictive tool for drinking water treatment. Environ. Sci. Technol. 34, 591–597. doi:10.1021/es990724e.

Bahnmüller, S., Loi, C.H., Linge, K.L., von Gunten, U., Canonica, S., 2015. Degradation rates of benzotriazoles and benzothiazoles under UV-C irradiation and the advanced oxidation process UV/H_2O_2. Water Res 74, 143–154. doi:10.1016/j.watres.2014.12.039.

Bolton, J.R., Stefan, M.I., 2002. Fundamental photochemical approach to the concepts of fluence (UV dose) and electrical energy efficiency in photochemical degradation reactions. Res. Chem. Intermed. 28, 857–870. doi:10.1163/15685670260469474.

Bolton, J.R., Stefan, M.I., Shaw, P.-S., Lykke, K.R., 2011. Determination of the quantum yields of the potassium ferrioxalate and potassium iodide–iodate actinometers and a method for the calibration of radiometer detectors. J. Photochem. Photobiol. A Chem. 222, 166–169. doi:10.1016/j.jphotochem.2011.05.017.

Brezonik, P.L., Fulkerson-Brekken, J., 1998. Nitrate-Induced Photolysis in Natural Waters: Controls on Concentrations of Hydroxyl Radical Photo-Intermediates by Natural Scavenging Agents. Environ. Sci. Technol. 32, 3004–3010. doi:10.1021/es9802908.

Buxton, G.V., Greenstock, C.L., Helman, W.P., Ross, A.B., 1988. Critical Review of rate constants for reactions of hydrated electrons, hydrogen atoms and hydroxyl radicals ($^{\cdot}OH/^{\cdot}O^{-}$) in Aqueous Solution. J. Phys. Chem. Ref. Data 17, 513–886. doi:10.1063/1.555805.

Canonica, S., Kohn, T., Mac, M., Real, F.J., Wirz, J., von Gunten, U., 2005. Photosensitizer Method to Determine Rate Constants for the Reaction of Carbonate Radical with Organic Compounds. Environ. Sci. Technol. 39, 9182–9188. doi:10.1021/es051236b.

Canonica, S., Meunier, L., von Gunten, U., 2008. Phototransformation of selected pharmaceuticals during UV treatment of drinking water. Water Res 42, 121–128. doi:10.1016/j.watres.2007.07.026.

Christensen, H., Sehested, K., Corfitzen, H., 1982. Reactions of hydroxyl radicals with hydrogen peroxide at ambient and elevated temperatures. J. Phys. Chem. 86, 1588–1590. doi:10.1021/j100206a023.

Crittenden, J.C., Hu, S., Hand, D.W., Green, S.A., 1999. A kinetic model for H_2O_2/UV process in a completely mixed batch reactor. Water Res 33, 2315–2328. doi:10.1016/S0043-1354(98)00448-5.

Donham, J.E., Rosenfeldt, E.J., Wigginton, K.R., 2014. Photometric hydroxyl radical scavenging analysis of standard natural organic matter isolates. Environ. Sci. Process. Impacts 16, 764. doi:10.1039/c3em00663h.

Elliot, A.J., Simsons, A.S., 1984. Rate constants for reactions of hydroxyl radicals as a function of temperature. Radiat. Phys. Chem. 24, 229–231. doi:10.1016/0146-5724(84)90056-6.

Froloff, N., Lloret, E., Martinez, J.-M., Faurion, A., 1998. Cross-adaptation and Molecular Modeling Study of Receptor Mechanisms Common to Four Taste Stimuli in Humans. Chem. Senses 23, 197–206. doi:10.1093/chemse/23.2.197.

Gerrity, D., Lee, Y., Gamage, S., Lee, M., Pisarenko, A.N., Trenholm, R.A., von Gunten, U., Snyder, S.A., 2016. Emerging investigators series: Prediction of trace organic contaminant abatement with UV/H_2O_2: Development and validation of semi-empirical models for municipal wastewater effluents. Environ. Sci. Water Res. Technol. 2, 460–473. doi:10.1039/c6ew00051g.

Haag, W.R., Hoigné, J., 1985. Photo-sensitized oxidation in natural water via .OH radicals. Chemosphere 14, 1659–1671. doi:10.1016/0045-6535(85)90107-9.

Hoigné, J., 1997. Inter-calibration of OH radical sources and water quality parameters. Water Sci. Technol. 35, 1–8. doi:10.1016/S0273-1223(97)00002-4.

Huber, M.M., Canonica, S., Park, G.Y., von Gunten, U., 2003. Oxidation of pharmaceuticals during ozonation and advanced oxidation processes. Environ. Sci. Technol. 37, 1016–1024. doi:10.1021/es025896h.

Hübner, U., Keller, S., Jekel, M., 2013. Evaluation of the prediction of trace organic compound removal during ozonation of secondary effluents using tracer substances and second order rate kinetics. Water Res 47, 6467–6474. doi:10.1016/j.watres.2013.08.025.

ISO/IEC, 2008. ISO/IEC Guide 98-3:2008. Uncertainty of measurement. Part 3: Guide to the expression of uncertainty in measurement (GUM:1995).

Jeong, J., Jung, J., Cooper, W.J., Song, W., 2010. Degradation mechanisms and kinetic studies for the treatment of X-ray contrast media compounds by advanced oxidation/reduction processes. Water Res 44, 4391–4398. doi:10.1016/j.watres.2010.05.054.

Keen, O.S., McKay, G., Mezyk, S.P., Linden, K.G., Rosario-Ortiz, F.L., 2014. Identifying the factors that influence the reactivity of effluent organic matter with hydroxyl radicals. Water Res 50, 408–419. doi:10.1016/j.watres.2013.10.049.

Kruithof, J.C., Kamp, P.C., Martijn, B.J., 2007. UV/H_2O_2 treatment: A practical solution for organic contaminant control and primary disinfection. Ozone-Science Eng 29, 273–280. doi:10.1080/01919510701459311.

Kwon, M., Kim, S., Yoon, Y., Jung, Y., Hwang, T.-M., Kang, J.-W., 2014. Prediction of the removal efficiency of pharmaceuticals by a rapid spectrophotometric method using Rhodamine B in the UV/H_2O_2 process. Chem. Eng. J. 236, 438–447. doi:10.1016/j.cej.2013.10.064.

Landesanstalt für Umwelt Baden-Württemberg, 2021. Daten- und Kartendienst der LUBW [WWW Document] URL https://udo.lubw.baden-wuerttemberg.de/public/pages/home/welcome.xhtml .

Lee, J., von Gunten, U., Kim, J.-H., 2020. Persulfate-Based Advanced Oxidation: Critical Assessment of Opportunities and Roadblocks. Environ. Sci. Technol. 54, 3064–3081. doi:10.1021/acs.est.9b07082.

Lee, Y., Gerrity, D., Lee, M., Bogeat, A.E., Salhi, E., Gamage, S., Trenholm, R.A., Wert, E.C., Snyder, S.A., von Gunten, U., 2013. Prediction of Micropollutant Elimination during Ozonation of Municipal Wastewater Effluents: Use of Kinetic and Water Specific Information. Environ. Sci. Technol. 47, 5872–5881. doi:10.1021/es400781r.

Lee, Y., Gerrity, D., Lee, M., Gamage, S., Pisarenko, A., Trenholm, R.A., Canonica, S., Snyder, S.A., von Gunten, U., 2016. Organic Contaminant Abatement in Reclaimed Water by UV/H_2O_2 and a Combined Process Consisting of O_3/H_2O_2 Followed by UV/H_2O_2: Prediction of Abatement Efficiency, Energy Consumption, and Byproduct Formation. Environ. Sci. Technol. 50, 3809–3819. doi:10.1021/acs.est.5b04904.

Lee, Y., Kovalova, L., McArdell, C.S., von Gunten, U., 2014. Prediction of micropollutant elimination during ozonation of a hospital wastewater effluent. Water Res 64, 134–148. doi:10.1016/j.watres.2014.06.027.

Lester, Y., Ferrer, I., Thurman, E.M., Linden, K.G., 2014. Demonstrating sucralose as a monitor of full-scale UV/AOP treatment of trace organic compounds. J. Hazard. Mater. 280, 104–110. doi:10.1016/j.jhazmat.2014.07.009.

Miklos, D.B., Hartl, R., Michel, P., Linden, K.G., Drewes, J.E., Hübner, U., 2018a. UV/H2O2 process stability and pilot-scale validation for trace organic chemical removal from wastewater treatment plant effluents. Water Res 136, 169–179. doi:10.1016/j.watres.2018.02.044.

Miklos, D.B., Remy, C., Jekel, M., Linden, K.G., Drewes, J.E., Hübner, U., 2018b. Evaluation of advanced oxidation processes for water and wastewater treatment – A critical review. Water Res 139, 118–131. doi:10.1016/j.watres.2018.03.042.

Miklos, D.B., Wang, W.L., Linden, K.G., Drewes, J.E., Hübner, U., 2019. Comparison of UV-AOPs (UV/H_2O_2, UV/PDS and UV/Chlorine) for TOrC removal from municipal wastewater effluent and optical surrogate model evaluation. Chem. Eng. J. 362, 537–547. doi:10.1016/j.cej.2019.01.041.

Minakata, D., Kamath, D., Maetzold, S., 2017. Mechanistic Insight into the Reactivity of Chlorine-Derived Radicals in the Aqueous-Phase UV–Chlorine Advanced Oxidation Process: Quantum Mechanical Calculations. Environ. Sci. Technol. 51, 6918–6926. doi:10.1021/acs.est.7b00507.

Minakata, D., Westerhoff, P., Crittenden, J.C., 2009. Development of a Group Contribution Method To Predict Aqueous Phase Hydroxyl Radical ($HO^{\bullet}$) Reaction Rate Constants. Environ. Sci. Technol. 43, 6220–6227. doi:10.1021/es900956c.

Morgan, M.G., Henrion, M., Small, M., 1990. Uncertainty: A Guide to Dealing with Uncertainty in Quantitative Risk and Policy Analysis. Cambridge University Press, Cambridge.

National Institute of Standards and Technology, 2002. NIST Standard Reference Database 40 [WWW Document]. URL https://kinetics.nist.gov/solution/ .

Pereira, V.J., Weinberg, H.S., Linden, K.G., Singer, P.C., 2007. UV degradation kinetics and modeling of pharmaceutical compounds in laboratory grade and surface water via direct and indirect photolysis at 254 nm. Environ. Sci. Technol. 41, 1682–1688. doi:10.1021/es061491b.

Plattner, J., Eugster, F., Svojitka, J., Wünsch, R., Gebhardt, J., Wülser, R., Wintgens, T., 2017. Removal of Micropollutants and Formation of Harmful By- Products in Advanced Oxidation Process with UV and H_2O_2 in Surface Water. In: N.N. (Ed.), 9th IWA Eastern European Young Water Professionals Conference, Budapest, 24-27 May 2017. IWA YWP, pp. 1–2.

Rahn, R.O., 1997. Potassium Iodide as a Chemical Actinometer for 254 nm Radiation: Use of Iodate as an Electron Scavenger. Photochem. Photobiol. 66, 450–455. doi:10.1111/j.1751-1097.1997.tb03172.x.

Real, F.J., Benitez, F.J., Acero, J.L., Sagasti, J.J.P., Casas, F., 2009. Kinetics of the Chemical Oxidation of the Pharmaceuticals Primidone, Ketoprofen, and Diatrizoate in Ultrapure and Natural Waters. Ind. Eng. Chem. Res. 48, 3380–3388. doi:10.1021/ie801762p.

Roback, S.L., Ishida, K.P., Plumlee, M.H., 2019. Influence of reverse osmosis membrane age on rejection of NDMA precursors and formation of NDMA in finished water after full advanced treatment for potable reuse. Chemosphere 233, 120–131. doi:10.1016/j.chemosphere.2019.05.259.

Rosenfeldt, E.J., Linden, K.G., 2007. The $R_{OH,UV}$ Concept to Characterize and the Model UV/H_2O_2 Process in Natural Waters. Environ. Sci. Technol. 41, 2548–2553. doi:10.1021/es062353p.

Rosenfeldt, E.J., Linden, K.G., Canonica, S., von Gunten, U., 2006. Comparison of the efficiency of $^{\bullet}OH$ radical formation during ozonation and the advanced oxidation processes O_3/H_2O_2 and UV/H_2O_2. Water Res 40, 3695–3704. doi:10.1016/j.watres.2006.09.008.

Scheideler, J., Lekkerkerker-Teunissen, K., Knol, T., Ried, A., Verberk, J.Q.J.C., Van Dijk, H.C., 2011. Combination of O3/H_2O_2 and UV for multiple barrier micropollutant treatment and bromate formation control – an economic attractive option. Water Pract. Technol. 6, 1–2. doi:10.2166/wpt.2011.0063.

Stefan, M.I., 2018. Advanced Oxidation Processes for Water Treatment. IWA Publishing, London doi:10.1021/jz300929x.

Tian, F.X., Xu, B., Lin, Y.L., Hu, C.Y., Zhang, T.Y., Gao, N.Y., 2014. Photodegradation kinetics of iopamidol by UV irradiation and enhanced formation of iodinated disinfection by-products in sequential oxidation processes. Water Res 58, 198–208. doi:10.1016/j.watres.2014.03.069.

Toth, J.E., Rickman, K.A., Venter, A.R., Kiddle, J.J., Mezyk, S.P., 2012. Reaction Kinetics and Efficiencies for the Hydroxyl and Sulfate Radical Based Oxidation of Artificial Sweeteners in Water. J. Phys. Chem. A 116, 9819–9824. doi:10.1021/jp3047246.

Trussell, R.S., Lai-Bluml, G., Chaudhuri, M., Johnson, G., 2019. Developing a regional recycled water program in Southern California. Water Pract. Technol. 14, 570–578. doi:10.2166/wpt.2019.042.

von Gunten, U., 2018. Oxidation Processes in Water Treatment: Are We on Track? Environ. Sci. Technol. 52, 5062–5075. doi:10.1021/acs.est.8b00586.

von Gunten, U., 2003. Ozonation of drinking water: Part II Disinfection and by-product formation in the presence of bromide. Water Res 37, 1469–1487.

von Gunten, U., Oliveras, Y., 1998. Advanced Oxidation of Bromide-Containing Waters: Bromate Formation Mechanisms. Environ. Sci. Technol. 32, 63–70. doi:10.1021/es970477j.

Wang, C., Rosenfeldt, E., Li, Y., Hofmann, R., 2020. External Standard Calibration Method To Measure the Hydroxyl Radical Scavenging Capacity of Water Samples. Environ. Sci. Technol. 54, 1929–1937. doi:10.1021/acs.est.9b06273.

Wenk, J.H., von Gunten, U., Canonica, S., 2011. Effect of Dissolved Organic Matter on the Transformation of Contaminants Induced by Excited Triplet States and the Hydroxyl Radical. Environ. Sci. Technol. 45, 1334–1340. doi:10.1021/es102212t.

Wolfram Alpha LLC, 2020. WolframAlpha [WWW Document]. URL https://www.wolframalpha.com/(accessed 6.2.20).

Wols, B.A., Harmsen, D.J.H., Beerendonk, E.F., Hofman-Caris, R.C.H.M., 2014. Predicting pharmaceutical degradation by UV (LP)/H_2O_2 processes: A kinetic model. Chem. Eng. J. 255, 334–343. doi:10.1016/j.cej.2014.05.088.

Wols, B.A., Harmsen, D.J.H., van Remmen, T., Beerendonk, E.F., Hofman-Caris, C.H.M., 2015a. Design aspects of UV/H2O2 reactors. Chem. Eng. Sci. 137, 712–721. doi:10.1016/j.ces.2015.06.061.

Wols, B.A., Harmsen, D.J.H., Wanders-Dijk, J., Beerendonk, E.F., Hofman-Caris, R.C.H.M., 2015b. Degradation of pharmaceuticals in UV (LP)/H2O2 reactors simulated by means of kinetic modeling and computational fluid dynamics (CFD). Water Res 75, 11–24. doi:10.1016/j.watres.2015.02.014.

Wols, B.A., Hofman-Caris, R.C.H.M., 2012. Review of photochemical reaction constants of organic micropollutants required for UV advanced oxidation processes in water. Water Res 46, 2815–2827. doi:10.1016/j.watres.2012.03.036.

Wols, B.A., Hofman-Caris, R.C.H.M., Harmsen, D.J.H., Beerendonk, E.F., 2013. Degradation of 40 selected pharmaceuticals by UV/H2O2. Water Res 47, 5876–5888. doi:10.1016/j.watres.2013.07.008.

Wünsch, R., Plattner, J., Cayon, D., Eugster, F., Gebhardt, J., Wülser, R., von Gunten, U., Wintgens, T., 2019. Surface water treatment by UV/H_2O_2 with subsequent soil aquifer treatment: impact on micropollutants, dissolved organic matter and biological activity. Environ. Sci. Water Res. Technol. 5, 1709–1722. doi:10.1039/C9EW00547A.

Yu, H., Park, M., Wu, S., Lopez, I.J., Ji, W., Scheideler, J., Snyder, S.A., 2019. Strategies for selecting indicator compounds to assess attenuation of emerging contaminants during UV advanced oxidation processes. Water Res 115030. doi:10.1016/j.watres.2019.115030.

Yu, H.W., Anumol, T., Park, M., Pepper, I., Scheideler, J., Snyder, S.A., 2015. On-line sensor monitoring for chemical contaminant attenuation during UV/H_2O_2 advanced oxidation process. Water Res 81, 250–260. doi:10.1016/j.watres.2015.05.064.

Zucker, I., Avisar, D., Mamane, H., Jekel, M., Hübner, U., 2016. Determination of oxidant exposure during ozonation of secondary effluent to predict contaminant removal. Water Res 100, 508–516. doi:10.1016/j.watres.2016.05.049.